

Multimessenger Pulsar Timing Array Constraints on Supermassive Black Hole Binaries Traced by Periodic Light Curves

Chengcheng Xin¹, Chiara M. F. Mingarelli^{2,3}, and Jeffrey S. Hazboun⁴

Columbia University, Department of Astronomy, 550 West 120th Street, New York, NY, 10027, USA; cx2204@columbia.edu

Center for Computational Astrophysics, Flatiron Institute, 162 Fifth Ave, New York, NY, 10010, USA

Department of Physics, University of Connecticut, 196 Auditorium Road, U-3046, Storrs, CT 06269-3046, USA

University of Washington Bothell, 18115 Campus Way NE, Bothell, WA 98011, USA

Received 2020 September 24; revised 2021 May 10; accepted 2021 May 13; published 2021 July 13

Abstract

Supermassive black hole binary systems (SMBHBs) emitting gravitational waves may be traced by periodic light curves. We assembled a catalog of 149 such periodic light curves, and using their masses, distances, and periods, predicted the gravitational-wave strain and detectability of each binary candidate using all-sky detection maps. We found that the International Pulsar Timing Array (IPTA) provides almost uniform sky coverage—a unique ability of the IPTA—and by 2025 will improve NANOGrav's current minimum detectable strain by a factor of 6 and its volume by a factor of 216. Moreover, IPTA will reach detection sensitivities for three candidates by 2025, and 13 by the end of the decade, enabling us to constrain the underlying empirical relations used to estimate supermassive black hole masses. We find that we can in fact already constrain the mass of a binary in Mrk 504 to $M < 3.3 \times 10^9 M_{\odot}$. We also identify 24 high-mass, high-redshift galaxies that, according to our models, should not be able to host SMBHBs. Importantly, the GW detection of even one of these candidates would be an essentially eternal multimessenger system, and identifying common false-positive signals from nondetections will be useful to filter the data from future large-scale surveys such as LSST.

Unified Astronomy Thesaurus concepts: Gravitational waves (678); Astrophysical black holes (98); Millisecond pulsars (1062); Supermassive black holes (1663); AGN host galaxies (2017); Active galactic nuclei (16); Gravitational wave astronomy (675); Gravitational wave sources (677); General relativity (641)

1. Introduction

Gravitational waves (GWs) emitted by supermassive black hole binary (SMBHBs) systems with periods of years to decades are expected to be the most powerful sources of GWs in the universe. Searches for individual SMBHBs can be aided by looking for periodic light curves in active galactic nuclei (AGN), which trace the SMBHB activity and serve as electromagnetic (EM) counterparts to these GW sources (e.g., Kauffmann & Haehnelt 2000; Goulding et al. 2018).

With decades of precision pulsar timing data, pulsar timing arrays (PTAs) are ready and able to make the first detection of low-frequency GWs (Burke-Spolaor et al. 2019). Ultra-stable radio millisecond pulsars are the best clocks in nature—deviations in their arrival times manifesting over years to decades can therefore signal the presence of passing low-frequency GWs (Hellings & Downs 1983).

Identifying the host galaxy of a SMBHB system would yield an essentially eternal multimessenger system—the black holes are millions of years from coalescence and would provide a treasure trove of science, such as direct evidence that the infamous final parsec problem is solved (Begelman et al. 1980) and clues as to how it was solved via the quantity of gas, stars, and residual eccentricity in the system (Milosavljević & Merritt 2001; Sesana 2013), as well as enabling us to probe General Relativity (see, e.g., O'Beirne et al. 2019).

Here, we have assembled a catalog of 149 periodic light curves that may trace SMBHB activity, including 111 SMBHB candidates from Catalina Real Time Transient Survey (CRTS; Graham et al. 2015a), 33 from the Palomar Transient Factory (PTF; Charisi et al. 2016), 3 from Pan-STARRS (Liu et al. 2019), OJ287 (Lehto & Valtonen 1996), and 3C66B (Sudou

et al. 2003; Arzoumanian et al. 2020a), though in the end we restrict our analysis to the Graham et al. (2015a) sample because we found that the other candidate binaries are too high-frequency to be detected.

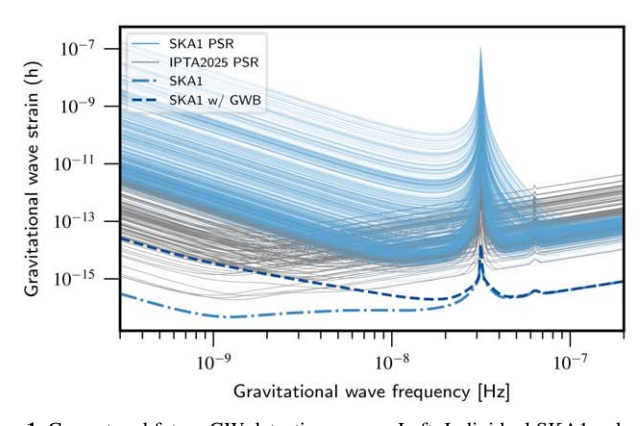
Using published binary parameters, we predict the GW strain of each binary candidate, and for the first time predict their time to detection by constructing all-sky detection maps to simulate the IPTA in 2025 (IPTA2025), Phase 1 of the Square Kilometre Array (SKA1), and its second phase (SKA2) using hasasia (Hazboun et al. 2019b; henceforth H19).

These public data, simulations and open-source codes will help to inform where to search for new pulsars to accelerate GW detection, and lead to targeted GW searches—making these searches more sensitive by at least factor of 2 (Arzoumanian et al. 2020a), or even more if the GW frequency is known.

2. Gravitational-wave Signals

Previously, the periodic light curves from Graham et al. (2015a), henceforth G15, were used by Sesana et al. (2018) to test the binary hypothesis: they showed that if all the AGN light curves were really SMBHBs, then the inferred cosmic population of SMBHBs would create a GW background that was in tension with the PTA upper limit at the time (Arzoumanian et al. 2018a). Kelley et al. (2019) also carried out simulations predicting that, statistically, five of the CRTS sources may contain genuine binaries.

We now have new tools we can apply directly to the CRTS sample for the first time: hasasia—a public code that can create continuous GW (CGW) detection sky maps—and new results from Arzoumanian et al. (2020a) showing that targeted



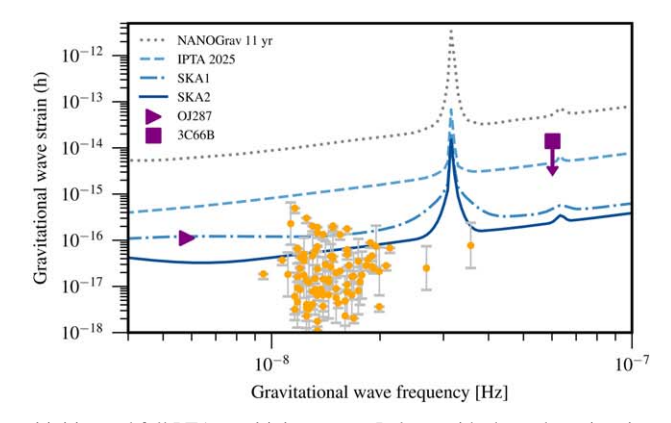


Figure 1. Current and future GW detection curves. Left: Individual SKA1 pulsar sensitivities and full PTA sensitivity curves. Pulsars with short observing time spans considerably increase the sensitivity at higher frequencies. The atypical flat bucket of the curve comes from the addition of pulsars with low rms and short time spans to the IPTA pulsars. An unresolved GW background with $A_{\text{GWB}} = 1.92 \times 10^{-15}$ deteriorates our sensitivity to individual SMBHBs by at most a factor \sim 3 for the lowest-frequency CRTS sources. Right: Truncated GW frequency regime relevant to CRTS sources (orange circles with $1 - \sigma$ error bars), OJ287, and 3C66B. The continuous curves are the S/N = 3 detection curves for NANOGrav, IPTA, and SKA1 and 2 experiments. We only plot candidates with strain $h > 10^{-18}$; GW strain less than this is unlikely to be detectable by PTAs.

searches can boost CGW sensitivity by at least a factor of two. Indeed, it is only now possible to rigorously investigate the detectability of each individual binary candidate's GW signal. The GW strain amplitude for a SMBHB is determined via

$$h = \frac{2\mathcal{M}_c^{5/3}(\pi f)^{2/3}}{D_L},\tag{1}$$

where $\mathcal{M}_c^{5/3} = q/(1+q)^2 M^{5/3}$ is the chirp mass, $M = M_1 + M_2$ is the total binary mass, $q = M_2/M_1 \leqslant 1$ is the mass ratio, D_L is the luminosity distance to the source, f is the observed GW frequency, and we let G = c = 1. Many of the mean BH mass estimates are reported in previous literature that identified periodic sources, e.g., G15, Charisi et al. (2016), and Liu et al. (2019). While G15 computed the strain in their Figure 10, they did not include errors on the total mass M (their error bars in Figure 10 are from varying $0.05 \leqslant q \leqslant 1.0$). This mass error is crucial for estimating the error on the strain h, since $h \propto M^{5/3}$, and is therefore even more important than the error on the mass ratio q.

We compute the SMBH masses as in G15, using the widths of $H\beta$ and Mg-II spectral emissions (Shen et al. 2008). We redo this calculation directly from SDSS spectra because G15 do not report mass errors, which are crucial for determining the uncertainties in h. In order to get a handle on these errors, we generate 160,000 Monte Carlo (MC) samples to create a distribution of the mass, M, and also sample in the ratio q from uniform distributions over the range 0.25 to a maximum of 1. The lower limit of q is somewhat arbitrary, but because the BH mass error dominates the uncertainty in h, the choice of the lower limit on a is of little consequence, as smaller values of a simply extend the lower value of the error bar on h. It is also interesting to note that, while the relativistic Doppler boost model is very important in some binary SMBH systems with small mass ratios (e.g., D'Orazio et al. 2015; Charisi et al. 2018), detecting this subcategory of SMBHB is difficult due to this small q value.

We interpret the peak of the distribution as the mean, h_0 , and the error bars are taken as one standard deviation (1σ) in the

mass distribution. While only 36 CRTS sources have the available SDSS spectra needed for this calculation, this method is generic and can be applied to a larger sample when spectra are available. We report all our mass calculations and their error estimates in Table 3.

The GW frequencies are obtained via reported binary orbital periods P, i.e., $f_{GW} = 2/P$. The luminosity distance D_L is computed via the redshift of the source, assuming cosmological parameters $H_0 = 0.7$ km Mpc⁻¹ s⁻¹ and $\Omega_m = 0.3$.

An important consideration for the detection of these individual SMBHB systems is the existence of a loud GW background (really a foreground), likely generated by the cosmic merger history of SMBHs. Currently, it is unknown what the true amplitude of this GW background is, though the most recent estimate is $A \sim 2 \times 10^{-15}$ (Arzoumanian et al. 2020b). Potential individual GW amplitudes in the data sets we investigate here are much lower than this, and at best, are at the level of some of the most conservative GW background models (Bonetti et al. 2018; Ryu et al. 2018; Sesana et al. 2018; Zhu et al. 2019). We therefore study the impact of this stochastic background signal on the detection of the individual SMBHB signals. On the left-hand side of Figure 1, we illustrate the effect of a stochastic GW background on the sensitivity to single sources as a separate noise source, though the background is obviously tied in with individual sources, especially at the detection threshold. The number of resolvable binaries in a single frequency bin—the so-called confusion limit for PTAs -varies in the literature from 4 (Babak & Sesana 2012) to 2N - 7 (Boyle & Pen 2012), where N is the number of pulsars in the PTA. Ever-evolving data analysis techniques (Bécsy & Cornish 2020) will allow individual sources to be pulled from the GWB as they become significant in more sensitive data sets. On the right-hand side of Figure 1, we show the strain amplitudes (orange dots) given by Equation 1 and the errors of h for the CRTS candidates, OJ287 and 3C66B, along with the detection curves for NANOGrav, IPTA, SKA1 and SKA2 with S/N = 3. The values of h can be compared with Figure 6 in Sesana et al. (2018), where they show the top ~half of the CRTS candidates with the strongest GW signals. In Section 6, we compare our top candidates with those in Sesana et al. (2018).

Since our catalog of candidate SMBHBs are mid-to-high GW frequency for PTAs, we also compute their GW frequency

We extract interactive spectra from SDSS Data Release 13 (DR13); https://www.sdss.org/dr13/spectro/ (Albareti et al. 2017).

evolution, \dot{f} ,

$$\dot{f} = \frac{96}{5} \pi^{8/3} \mathcal{M}_c^{5/3} f^{11/3}. \tag{2}$$

The expert reader will notice that small values of \dot{f} mean that the Earth term and the pulsar term lie in the same GW frequency bin, and will thus double a pulsar's residual. This has been taken into account in hasasia (see H19).

3. Electromagnetic Counterparts

Hydrodynamical simulations have demonstrated that bright quasar variability can be modulated periodically by the orbital period of the binary SMBH, due to perturbations by the surrounding gas in the circumbinary accretion disk; see, e.g., Roedig et al. (2014); Farris et al. (2014a); D'Orazio et al. (2016), and references therein.

A promising observational approach to identify SMBHBs in the optical bands is to search for quasars with periodic variability. One of the first candidate SMBHBs, OJ287, was identified with variable observed luminosity fluctuations in the form of repeating outbursts occurring every ~12 yr (Lehto & Valtonen 1996; Laine et al. 2020). Another prominent object is an unequal-mass SMBHB candidate in quasar PG1302-102. It emerged from a systematic search in CRTS for its quasi-sinusoidal optical variability (Graham et al. 2015b), possibly due to the fact that the emissions from its mini-disk are Doppler-boosted (D'Orazio et al. 2015; Xin et al. 2020).

Infrared (IR) variability can also be caused by an SMBHB heating its surrounding dust torus; see, e.g., Antonucci (1993) and Krolik & Begelman (1988). In fact, Jun et al. (2015) and D'Orazio & Haiman (2017) implemented the IR reverberation modeling to a Doppler-boosted system, PG1302-102, and reproduced its periodicity in the optical light curve in IR wavelength. As such, candidate binaries may further benefit from follow-up measurements by the James Webb Space Telescope.

In addition to periodicity, spectral signatures across optical, UV, and X-ray bands are widely used to differentiate binary SMBHs from normal AGNs powered by single SMBHs. Merging binary SMBHs likely have different X-ray spectral profiles from isolated SMBHs, including harder X-ray spectra (Farris et al. 2014b; Roedig et al. 2014; Ryan & MacFadyen 2017). Of particular relevance is Saade et al. (2020), who measured X-ray spectra of seven CRTS candidates within the Chandra X-ray energy range and computed their optical/UV-to-X-ray spectral indices. While their spectra showed no difference from the broader AGN population with a purported single SMBH, they are careful to note this is not entirely unexpected: in some theoretical models (e.g., Roedig et al. 2014), thermal X-ray profiles can only distinguish binaries separated by $100 \, {\rm r_g}$, where $r_g = GM \, c^{-2}$ is the gravitational radius.

Interestingly, Saade et al. (2020) identified HS 1630+2355 (also known as FBQS J163302.6+234928) as the only AGN in their sample that could host an SMBHB, since its semimajor axis is $a \sim 57 \, r_g$, making it a tantalizing SMBHB candidate, which we highlight moving forward.

4. Forecasting PTA Capabilities

In addition to cataloging current candidate SMBHB systems, we estimate when these binaries may be detected. Using H19's

open-source Python package hasasia, we assess the current sensitivity of NANOGrav and forecast the sensitivity of future PTA experiments. For resolvable individual signals from SMBHBs, this involves using a matched filter statistic and building an effective strain-noise power spectral density (interpreted as the sensitivity) using the sky location, detector response functions, and noise parameters of the pulsars. The detection thresholds are then calculated using the expectation value of the S/N for a circular binary given the sensitivity. There are many subtleties involved with calculating a PTA's sensitivity to various GW sources, and the interested reader is encouraged to refer to H19 for details necessarily left out here.

There are a number of statistics in the literature (Babak & Sesana 2012; Ellis et al. 2012; Taylor et al. 2014) developed for single-source (CGW) searches in PTA data sets. Here, we use the S/N from Hazboun et al. (2019b), as it was developed with calculations of generic sky sensitivities in mind. In our forecasts, we have used the full rms errors quoted by current PTA data release papers, but have avoided explicitly injecting any time-correlated (red) noise into these pulsars, since it is unclear how much of the red noise currently observed in PTA pulsars is due to the stochastic background of GWs and how much is due to intrinsic spin noise. It is also likely that in the SKA era, if red noise models are not sufficient for PTA use, then it will be feasible to avoid the small number of millisecond pulsars (Arzoumanian et al. 2018b) with large red noise amplitudes.

The NANOGrav 11 yr detection curve is based on the noise parameters in Arzoumanian et al. (2018b). The IPTA2025 curve uses the pulsars and noise parameters from Perera et al. (2019) as a starting place, and builds the array by adding four pulsars per year with rms values of 300 ± 100 ns. In order to add four IPTA pulsars per year to those in Perera et al. (2019), we use the sky positions of the current pulsars to build empirical distributions for drawing new pulsar positions. The rms values for the pulsars are drawn from a truncated normal distribution with mean and standard deviation of $300 \text{ ns} \pm 100 \text{ ns}$, truncated at 10 ns and 600 ns. The cadences are pulled from an empirical distribution based on those in Arzoumanian et al. (2018b) and Perera et al. (2019), where any new pulsar with an rms less than 300 ns is observed weekly.

The SKA sensitivity estimates are based on projected IPTA data with a large addition of pulsars distributed according to the planned SKA MID and LOW surveys in the first few years of the SKA1 (Keane et al. 2015). Both conservative and more optimistic estimates for SKA1 and 2 are included here. The SKA LOW survey will concentrate on regions further than $\pm 5^{\circ}$ from the galactic plane, while the SKA MID survey will concentrate on regions within 10° of the galactic plane (Keane et al. 2015). We assume that 15% of the millisecond pulsars discovered will be suitable for PTAs, meaning that SKA1 will have ~ 675 millisec pulsars and SKA2 will have 120 more. All pulsars in IPTA2025 are used in the SKA with extended baselines from IPTA DR2 (Perera et al. 2019), as it is assumed that any SKA PTA will be based in large part on the extensive data sets from other PTAs.

We offer both optimistic and conservative outlooks for constraining SMBHB candidate masses in Table 1 (detection prospects in Table 2). Our conservative sensitivity projections use the same empirical distribution of rms errors as are used to build IPTA2025, while the optimistic sensitivities are built using a distribution more in line with the pulsars' rms being

Table 1
Top 13 Periodic SMBHB Candidates Ranked by Strain Upper Limit (UL; $h_{1\sigma}$), Where the Mass Can Be Constrained by SKA2 (11 in *CRTS* Plus OJ287 and 3C66B)

Object Name	RA	Dec	f_{GW} [Hz]	$\log(M)$ $[M_{\odot}]$	Strain $h_{1\sigma}$	NG <i>ρ</i> , 11-yr	IPTA ρ , 2025	SKA1 ρ, 2030	SKA2 ρ , 2034+
3C66B*	02 23 11.5	+42 59 30	6.04E-08	9.08	1.40E-14	1.60	15.7	82.2(35.1)	164(69.5)
HS 1630+2355	16 33 02.7	$+23\ 49\ 28.8$	1.13E-08	9.86	6.25E-16	0.9	4.86	18.32(8.19)	40.45(16.51)
SDSS J164452.71+4307	16 44 52.7	+43 07 52.9	1.16E-08	10.15	4.94E-16	0.65	3.67	13.77(6.26)	30.82(12.73)
SDSS J114857.33+1600	11 48 57.4	$+16\ 00\ 22.7$	1.25E-08	9.9	3.03E-16	0.22	1.39	6.88(2.74)	16(6.27)
HS 0926+3608	09 29 52.1	+35 54 49.6	1.48E-08	9.95	2.04E-16	0.08	0.74	4.29(1.66)	9.52(3.68)
SDSS J092911.35+2037	09 29 11.3	$+20\ 37\ 09.2$	1.30E-08	9.92	2.02E-16	0.07	0.87	4.43(1.73)	10.89(4.17)
SDSS J133516.17+1833	13 35 16.1	+18 33 41.8	1.34E-08	9.76	1.91E-16	0.18	1.00	4.67(1.92)	9.7(3.87)
SDSS J140704.43+2735	14 07 04.5	+27 35 56.3	1.48E-08	9.94	1.89E-16	0.17	0.95	4.50(1.86)	8.90(3.56)
SDSS J134855.27-0321	13 48 55.3	-3 21 41.4	1.62E-08	9.89	1.78E-16	0.14	0.8	4.09(1.64)	7.95(3.17)
SDSS J160730.33+1449	16 07 30.3	$+14\ 49\ 04.2$	1.34E-08	9.82	1.45E-16	0.17	0.95	3.97(1.71)	7.94(3.22)
SDSS J131706.19+2714	13 17 06.2	$+27\ 14\ 16.7$	1.39E-08	9.92	1.34E-16	0.11	0.63	3.08(1.26)	6.50(2.57)
SNU J13120+0641	13 12 04.7	+06 41 07.6	1.55E-08	9.14	1.33E-16	0.1	0.57	2.98(1.19)	5.97(2.37)
OJ287	08 54 48.9	+20 06 31	5.82E-09	10.26	1.11E-16	0.06	1.05	1.92(1.33)	9.69(3.69)

Notes. For detection claims, we use h_0 , Table 2. A further 15 candidates have marginal $S/N \sim 3$ but are not shown here. The last four columns report the S/N (ρ) on the $1-\sigma$ strain value for current and future PTA experiments. In the last two columns, the S/N values are listed as optimistic(conservative). Importantly, Arzoumanian et al. (2020a) find that strain ULs improve by a factor of at least two in targeted GW searches, which we do not take into account here. *For 3C66B, $h_{1\sigma}$ is the 95% UL from Arzoumanian et al. (2020a).

 Table 2

 Top 13 Periodic SMBHB Candidates, Ranked by the Mean Strain (h_0), which can be Detected or Constrained by SKA2 (11 in CRTS Plus OJ287 and 3C66B)

Object Name	RA	Dec	f_{GW} [Hz]	$\log(M)$ $[M_{\odot}]$	Strain h_0	NG ρ , 11-yr	IPTA ρ , 2025	SKA1 ρ, 2030	SKA2 ρ , 2034+
3C66B*	02 23 11.5	+42 59 30	6.04E-08	9.08	7.2E-15	0.82	8.06	42.27 (18.06)	84.59 (35.72)
HS 1630+2355	16 33 02.7	$+23\ 49\ 28.8$	1.13E-08	9.86	2.29E-16	0.33	1.78	6.71(3.00)	14.82(6.05)
SDSS J164452.71+4307	16 44 52.7	+43 07 52.9	1.16E-08	10.15	4.94E-16	0.65	3.67	13.77(6.26)	30.82(12.73)
SDSS J114857.33+1600	11 48 57.4	$+16\ 00\ 22.7$	1.25E-08	9.9	3.02E-16	0.22	1.39	6.86(2.73)	15.95(6.25)
HS 0926+3608	09 29 52.1	+35 54 49.6	1.48E-08	9.95	2.04E-16	0.08	0.74	4.29(1.66)	9.52(3.68)
SDSS J092911.35+2037	09 29 11.3	$+20\ 37\ 09.2$	1.30E-08	9.92	2.02E-16	0.07	0.87	4.43(1.73)	10.89(4.17)
SDSS J133516.17+1833	13 35 16.1	+18 33 41.8	1.34E-08	9.76	1.91E-16	0.18	1.00	4.67(1.92)	9.7(3.87)
SDSS J140704.43+2735	14 07 04.5	+27 35 56.3	1.48E-08	9.94	1.89E-16	0.17	0.95	4.50(1.86)	8.9(3.56)
SDSS J134855.27-0321	13 48 55.3	-3 21 41.4	1.62E-08	9.89	1.78E-16	0.14	0.80	4.09(1.64)	7.95(3.17)
SDSS J160730.33+1449	16 07 30.3	$+14\ 49\ 04.2$	1.34E-08	9.82	1.44E-16	0.17	0.94	3.94(1.69)	7.88(3.2)
SDSS J131706.19+2714	13 17 06.2	$+27\ 14\ 16.7$	1.39E-08	9.92	1.34E-16	0.11	0.63	3.08(1.26)	6.50(2.57)
SNU J13120+0641	13 12 04.7	+06 41 07.6	1.55E-08	9.14	1.33E-16	0.10	0.57	2.98(1.19)	5.97(2.37)
OJ287	08 54 48.9	+20 06 31	5.82E-09	10.26	1.11E-16	0.06	1.05	1.92(1.33)	9.69(3.69)

Notes. A further four candidates have marginal $S/N \sim 3$, but are not shown here. The last four columns report the S/N (ρ) on h_0 —the maximum *a posteriori* strain value—for current and future PTA experiments. The last two columns list the *optimistic(conservative)* S/N values. The S/N calculations here do not include the additional factor of two one achieves from a targeted search (Arzoumanian et al. 2020a). *For 3C66B, h_0 is calculated in Arzoumanian et al. (2020a).

"jitter limited" (Shannon et al. 2014; Lam et al. 2016, 2019), with mean and standard deviation of $100 \text{ ns} \pm 30 \text{ ns}$, truncated at 9 ns and 201 ns. In general, we leave the rms values of the adopted IPTA pulsars unchanged, except for PSR J1640 +2224, which is extremely close in sky position to HS 1630 +2355, and the two best timers in this region of the sky, PSR J1909-3744 and PSR J1713+0747. These three pulsars are assumed to be observed by the SKA and their rms values for the time spans considered here are set to the jitter values from Lam et al. (2019).

All PTA detection curves are presented as S/N = 3 thresholds on the GW strain.⁶ This is the threshold set by the PTA community for detection of single sources in the nanohertz band. These forecasts represent only a limited number of the many permutations one could postulate, hence the Jupyter

Notebooks used to make these projections are available on GitHub.

4.1. Special Considerations for Multimessenger Signals

When a periodic light curve or another EM tracer for an SMBHB system is identified, there are some concrete steps to take to increase a PTA's sensitivity to the candidate GW source.

It is our good fortune that the top two potential SMBHB host galaxies in Table 1 lie either in, or very close to, both the European PTA (EPTA) and NANOGrav's most sensitive region of the sky (Babak et al. 2016; Aggarwal et al. 2019). This already improves their detection prospects. Moreover, if a pulsar is close to the sky location of a potential SMBHB system, one also gains a factor of a few in sensitivity from the pulsar detector response function. We can take concrete steps to increase the S/N (ρ) of a potential GW candidate: $\rho \propto \langle NTc/\sigma^2 \rangle^{1/2}$, where for simplicity the N pulsars have the

There is a factor of 2 difference in the definition of h_0 between H19 and this manuscript, which has been taken into account for all of our calculations.

same intrinsic properties, T is the length of the data set, c is the cadence of the observation, and σ is the white noise rms (see, e.g., Arzoumanian et al. 2018b). We can therefore increase the S/N by increasing the number of pulsars, as well as the pulsar observing cadence c, and spending more time on observing these in an effort to decrease the rms white noise value σ (Burt et al. 2011; Mingarelli et al. 2017; Lam 2018). Moreover, combining pulsar data sets under the auspices of the IPTA is an excellent way to readily increase a pulsar's total observing time T and cadence c.

Furthermore, Arzoumanian et al. (2020a) show that targeted GW searches increase NANOGrav's GW sensitivity by at least a factor of two—more if there is GW frequency information.

Some things are left to chance: both NANOGrav and EPTA show uneven CGW sensitivity on the sky due to the largely anisotropic distribution of pulsars, and their uneven timing properties. If we are fortunate, the source will lie in an area of high sensitivity. Moreover, the antenna beam pattern (or detector response function) of a pulsar in direction \hat{p} to a GW is $\propto 1/(1+\hat{\Omega}\cdot\hat{p})$, where $\hat{\Omega}$ is the direction of GW propagation. This response function has been well-studied, and is clearly maximal for CGW sources in direction $-\hat{\Omega}$, since the denominator becomes small as $-\hat{\Omega}\to\hat{p}$. At exactly $\hat{\Omega}\cdot\hat{p}=-1$, the response is zero due to surfing effects (Baskaran et al. 2008; Chamberlin & Siemens 2012; Mingarelli & Sidery 2014). If we are very fortunate, the GW source will not only lie in a sensitive sky region, but also be closely aligned with a pulsar.

5. Unlikely Binaries in CRTS

Mingarelli et al. (2017) computed the probability of a galaxy hosting a SMBHB system emitting nanohertz GWs:

$$P_{\text{merger}} = \frac{t_c}{T_z} \int_{0.25}^{1} d\mu_* \frac{dN}{dz} (M_*, z, \mu_*) T_z, \tag{3}$$

where $t_c = 5/256(\pi f)^{-8/3}\mathcal{M}_c^{-5/3}$, dN/dz is the cumulative galaxy-galaxy merger rate (Rodriguez-Gomez et al. 2015), μ_* is the stellar mass ratio of the parent galaxies, and T_z is the estimated binary lifetime.

Briefly, this probability is the product of the probability of two factors: the existence of a pair of SMBHs in the galaxy resulting from a galaxy merger (the integrand in Equations (3)), and the probability that this binary is emitting nanohertz GWs, t_c/T_z . Here, the binaries overcome the final parsec problem (Begelman et al. 1980) via stellar hardening (Quinlan 1996).

We use the public software Nanohertz GWs (Mingarelli 2017) to compute this probability for all the AGN in our sample. Since the AGN light-curve catalog we assembled is not complete, we can only provide a relative ranking of the probability of a given AGN hosting an SMBHB.

Systems at higher redshift may contain more gas, hence the SMBHBs may overcome the final parsec problem by gas interactions in addition to stellar hardening (e.g., Sesana 2013; Tiede et al. 2020). The gas and stellar three-body interactions may also lead to large binary eccentricities, which is a subject for future study and could also help to solve the final parsec problem. A follow-up paper will include more such solutions to the final parsec problem.

Table 3
List of 36 SMBHB Candidates with BH Total Mass Error Estimates Obtained with the Width of Broadline Spectral Emissions (Shen et al. 2008), and the Rate of Change in Their GW Frequencies, in Hz per Year

	<u>.</u>	
Object Name	$\log(M/M_{\odot})$	$\dot{f}_{GW}[\mathrm{Hz}\;\mathrm{yr}^{-1}]$
HS 1630+2355	9.74 ± 0.26	8.98E-04
SBS 0920+590	9.20 ± 0.29	6.95E-04
FBQS J081740.1+23273	9.38 ± 0.28	1.40E-03
SDSS J131706.19+2714	9.35 ± 0.28	5.32E-04
SDSS J155449.11+0842	9.21 ± 0.28	4.87E-05
SDSS J104430.25+0518	9.26 ± 0.29	4.81E-05
SDSS J143621.29+0727	9.22 ± 0.28	3.85E-04
SDSS J133127.31+1824	9.21 ± 0.30	2.83E-04
HS 0946+4845	9.02 ± 0.29	1.65E-05
SDSS J150450.16+0122	9.18 ± 0.29	1.34E-04
SDSS J144755.57+1000	8.95 ± 0.29	6.08E-04
SDSS J083349.55+2328	9.01 ± 0.30	5.08E-03
SDSS J091554.50+3529	9.02 ± 0.3	4.90E-05
SDSS J121018.66+1857	9.12 ± 0.29	2.73E-05
SDSS J082827.84+4003	9.13 ± 0.29	1.19E-04
CSO 67	9.02 ± 0.29	1.23E-04
SDSS J114438.34+2626	9.03 ± 0.28	5.86E-05
SDSS J121457.39+1320	8.93 ± 0.30	9.96E-05
SDSS J082121.88+2508	8.98 ± 0.30	6.33E-04
SDSS J152157.02+1810	8.86 ± 0.31	5.58E-07
SDSS J133654.44+1710	8.77 ± 0.31	3.47E-05
SDSS J224829.47+1444	8.75 ± 0.31	8.85E-05
SDSS J124044.49+2310	8.74 ± 0.30	1.58E-04
SDSS J221016.97+1222	8.93 ± 0.29	7.35E-05
QNZ3:54	8.65 ± 0.31	5.30E-06
SDSS J115346.39+2418	8.77 ± 0.31	5.76E-05
SDSS J115141.81+1421	8.70 ± 0.31	6.10E-05
SDSS J082716.85+4905	8.66 ± 0.31	5.21E-07
SDSS J132103.41+1237	8.69 ± 0.32	6.78E-05
SDSS J154409.61+0240	8.86 ± 0.30	1.42E-05
SDSS J170616.24+3709	8.55 ± 0.31	4.45E-06
SDSS J133807.69+3602	8.61 ± 0.32	5.39E-06
SDSS J103111.52+4919	8.64 ± 0.30	1.61E-05
SDSS J104758.34+2845	8.54 ± 0.30	2.12E-06
SDSS J130040.62+1727	8.62 ± 0.30	2.48E-05
SDSS J082926.01+1800	8.49 ± 0.30	1.28E-05

Note. A mass uncertainty of $\sim\pm0.3$ on log-scale (shown in Column 2) results in a wide window of possible mass values for any candidate above—the actual mass can be a factor of 2 larger $(10^{+0.3})$ or 50% smaller $(10^{-0.3})$ than the mean RH mass

6. Results

Of the 111 CRTS sources, mass estimates are available for 98. We therefore compute the strain for 136 SMBHB candidates identified in the CRTS, PTF, and Pan-STARRS1 surveys, alongside individual quasars OJ287 and 3C66B, and compare the strains with current and future PTA detection curves. None of the PTF and Pan-STARRS1 candidates are detectable by SKA2, because these candidates generally must have larger masses and very low GW frequencies to be detectable by any PTA. Therefore, we focus our attention on CRTS.

A multimessenger signal could be an important test of GR by comparing the change in the observed EM period and the change in the GW frequency, akin to the Hulse-Taylor binary (Hulse & Taylor 1975). As such, we compute the GW frequency derivative, $\dot{f}_{\rm gw}$, Equations (2), for all the SMBHB candidates. We find that most of the CRTS candidates would have a GW frequency shift of $\sim 10^{-4}$ nHz yr⁻¹, and would

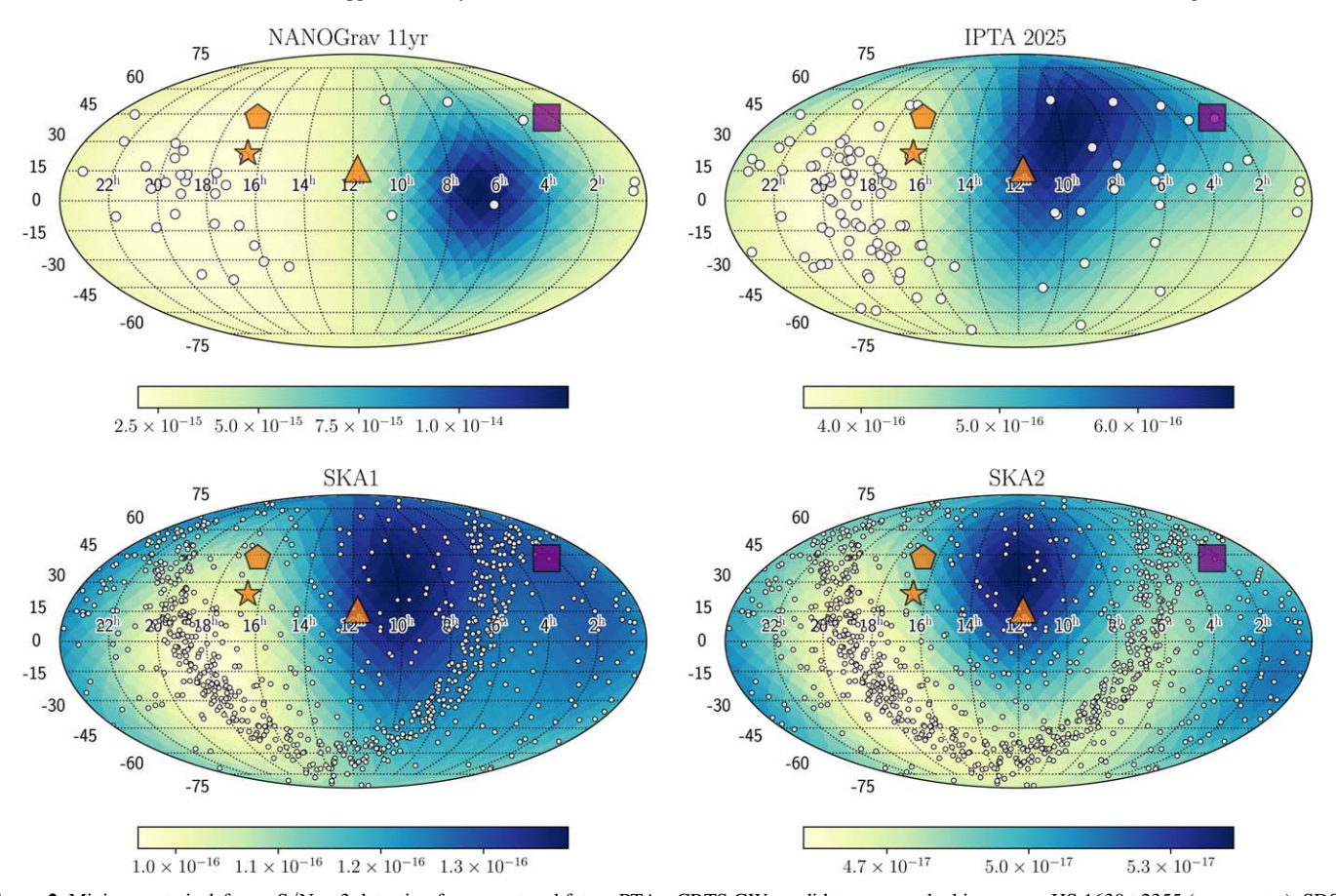


Figure 2. Minimum strain h for an S/N = 3 detection for current and future PTAs. CRTS GW candidates are marked in orange: HS 1630+2355 (orange star), SDSS J164452.71+4307 (orange pentagon), and SDSS J114857.33+1600 (orange triangle) are shown over the detection threshold of S/N = 3 for the NANOGrav 11 yr data set, and the hasasia-modeled IPTA2025, SKA1, and SKA2 PTAs at 11.8 nHz. The purple square is 3C66B, possessing the largest S/N in Table 1. While not in this frequency bin, the relative differences and proximity to pulsars are useful for comparison. Pulsars are small white circles, with their locations determined by planned SKA LOW and MID surveys (Keane et al. 2015).

therefore not be detectable. We report the list of computed \dot{f} values in Table 3. However, we find that for 3C66B $\dot{f}_{\rm gw}=0.14~{\rm nHz\,yr^{-1}}$. Since Sudou et al. (2003)'s claim that 3C66B is a binary with an orbital period of $1.05\pm0.03~{\rm yr}$, the source should have evolved from $60.4~{\rm nHz}$ to $62.8~{\rm nHz}$ over the last 17 yr if it were indeed an SMBHB system. Today, it would have a period of $P=2/62.8~{\rm nHz}=1.01~{\rm yr}$ —an evolution of 15 days since the initial measurement. The error on the original period is about 11 days, so new EM measurements may prove to be illuminating.

Importantly, galaxy 3C66B's detection prospects leap by almost an order of magnitude from the 11 yr data constraints (Arzoumanian et al. 2020a) to IPTA2025 (see Table 2). Much of this increase in detectability is due to the IPTA's enhanced sky coverage, even over IPTA DR2. Similar to the estimates for PSR J1640+2224, PSR J0218+4232's proximity to 3C66B makes it an ideal target for longer observing periods and a high-cadence timing campaign.

We also find that we will be able to constrain SMBHB masses earlier than we can detect them, so we report two strain values: $h_{1\sigma}$, which is the 1σ upper limit value of the strain (Table 1), and h_0 , which is the maximum a posteriori value of the strain (Table 2). When we refer to constraints on the mass, we refer to $h_{1\sigma}$ —this is the point where we can start to constrain the mass upper limits—and for detection claims, we refer to h_0 . While the mass ratio q will be uncertain, these upper bounds on strain are dominated by total mass uncertainty.

In Figure 1, we show the strain for the CRTS candidates, and for 37 of these, we can compute the mass from SDSS spectra in order to compute the strain error bars, Table 3 (spectra were not immediately available for the remaining candidates). If the upper error bar touches the S/N=3 detection curve with $h_{1\sigma}$, we claim that we can constrain the binary's total mass. We also show how important the new SKA pulsars will be for PTAs—even with short timing baselines, these new pulsars lead to significant improvements in detection prospects at mid-to-high GW frequencies.

It is encouraging that all candidates except the weakest one, SDSS J081617.73+293639.6, in Table 1 of Sesana et al. (2018) (see also their Figure 6) are also in our Table 1. While they rank their objects by strain from one Monte Carlo realization and compute the resulting amplitude of the gravitational wave background, we compute the strain over $\sim\!10^5$ realizations and subsequently estimate the time to detection of these SMBHB candidates.

The sky and polarization averaged detection curve does not, however, give the complete picture, since GW sensitivity is also a function of sky position and overall alignment with well-timed millisecond pulsars. We therefore use hasasia to generate future PTA detection sky maps (Figure 2). We find that the continuous GW sensitivity is largely smoothed out over the sky by going from a single PTA (here, NANOGrav) to the IPTA, as expected but never concretely shown. It is also interesting to note the residual effect the IPTA data have on

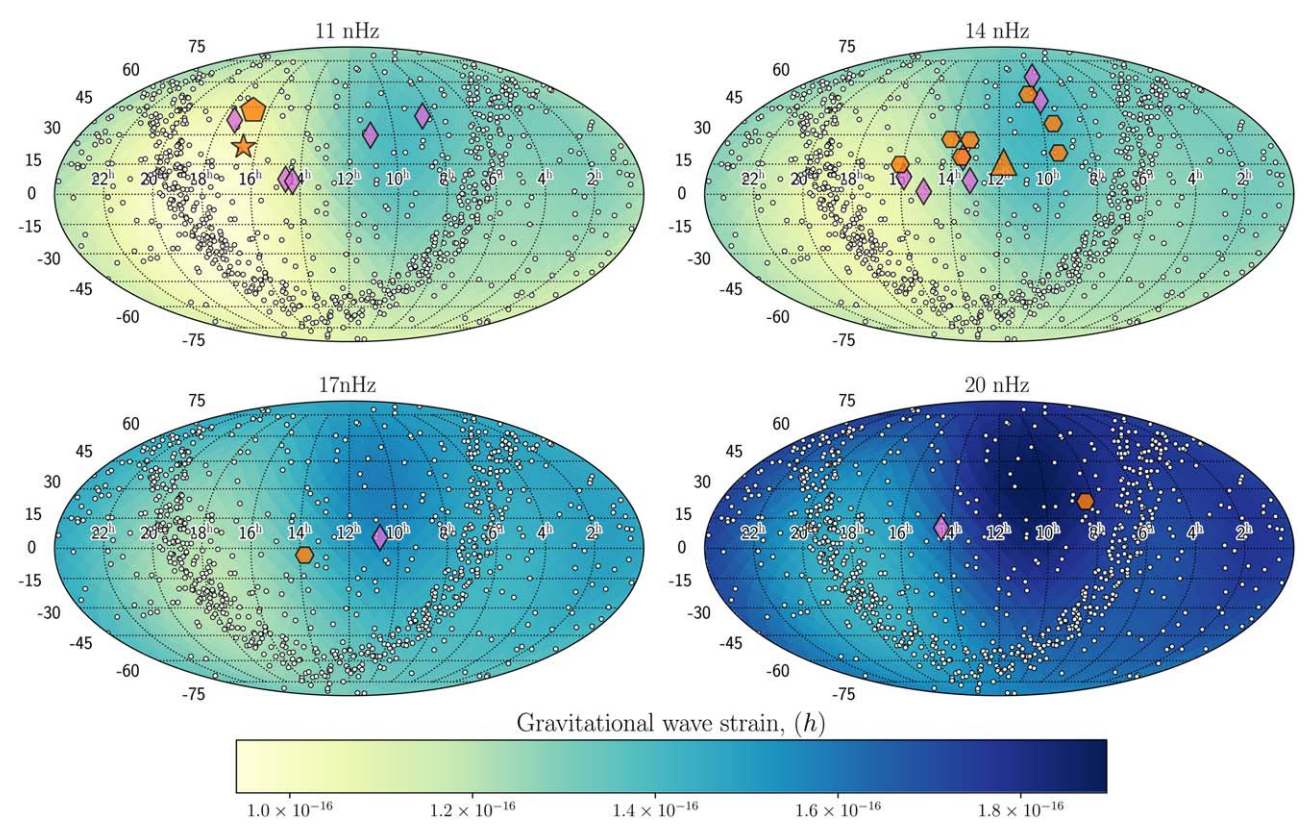


Figure 3. Minimum strain for S/N = 3 detection for SKA1. The candidates HS 1630+2355 (orange star), SDSS J164452.71+4307 (orange pentagon), and SDSS J114857.33+1600 (orange triangle) are again highlighted over the detection threshold for SKA1 at four different frequency bins with pulsars as white circles. The orange hexagons show the sources whose 1σ masses will be limited in SKA1. The light purple diamonds show the sky position of the remaining CRTS sources from Table 1.

SKA1's sky map, inducing a slight preference for GW observations in the northern hemisphere, while this is virtually washed out by SKA2.

Importantly, NANOGrav's most sensitive area improves by a factor of 6 in the strain, or a factor of 216 in volume, between the 11 yr data and our projections for IPTA2025. Moving from IPTA2025 to SKA1 yields a further factor of 4 improvement for the strain in 5 yr, and going from SKA2 to from SKA1 yields another factor of 2 in strain sensitivity. Improvements between SKA1 and SKA2 are modest because many of the pulsars in the SKA MID and LOW surveys will likely be found by 2034 and beyond, according to Keane et al. (2015).

In Table 1, we rank the selected CRTS sources from highest 1σ strain upper limit to lowest. Using $h_{1\sigma}$, we find that 3C66B, SDSS J164452.71+4307, and HS 1630+2355 should have S/N > 3 with IPTA2025 data if they are real binaries. If not detected, we can start to constrain their masses, and eventually rule out these AGN as SMBHB host galaxies. SKA1 will constrain 12, and SKA2 will constrain 28 SMBHB candidates masses. We also find that IPTA2025 can detect 2 sources (3 if we include the factor of 2 from Arzoumanian et al. 2020a), SKA1 can detect 12, and SKA2 can detect 17 sources. Our findings are summarized in Tables 1 and 2, and Figures 2 and 3.

We also note that SDSS J114857.33+1600's detection prospects improve by a factor of five from IPTA2025 to SKA1 in five years—this is due to the large increase of low-rms

pulsars added by preliminary SKA MID and LOW surveys (Keane et al. 2015) and timed for only up to four years. This large increase in sensitivity over a short time is also illustrated and explained by Figure 1.

HS 1630+2335 and Mrk 504 both show periodicity in the optical (Figure 4) and are not ruled out in X-ray (see Saade et al. 2020 and references therein), making them very interesting SMBHB candidates for continued investigations. Quite serendipitously, HS 1630+2335 is closely aligned with PSR J1640+2224, which is already a target in NANOGrav's high-cadence timing campaign. PSR J1640+2224's residuals have decreased by a factor of three since the first NANOGrav data release, making this pulsar a key tool to detect GWs from HS 1630+2335, or to rule it out as a true SMBHB. According to our calculations, the S/N based on $h_{1\sigma}$ of HS 1630+2335 in the NG 11 yr data is \sim 0.9. As a simplifying assumption, we assume all the signal comes from PSR J1640+2224 (a detection will require multiple pulsars). Moving from the 11 yr to 12.5 yr data will quadruple the cadence, and the rms of the residuals is half of the 11 yr value, ergo the S/N would improve by a factor of ~ 3 . Moreover, a dedicated search for this source in the NANOGrav 12.5 yr data would give an additional factor of 2 in sensitivity, with the admittedly optimistic potential of making a detection at $h_{1\sigma}$ with S/N \sim 5—comparable to the sensitivity of IPTA2025.

We show Mrk 504's EM periodicity in Figure 4, along with the photometry extracted from CRTS. It has a 10 yr data baseline, and we find its period to be 1410 days, very close to the Graham et al. (2015a) value of 1408 days. The data, ending at MJD 56580, could therefore cover about two binary orbital

⁷ Note that the strain calculations for SDSS J164452.71+4307 do not have mass errors, therefore $h_0 \approx h_{1\sigma}$.

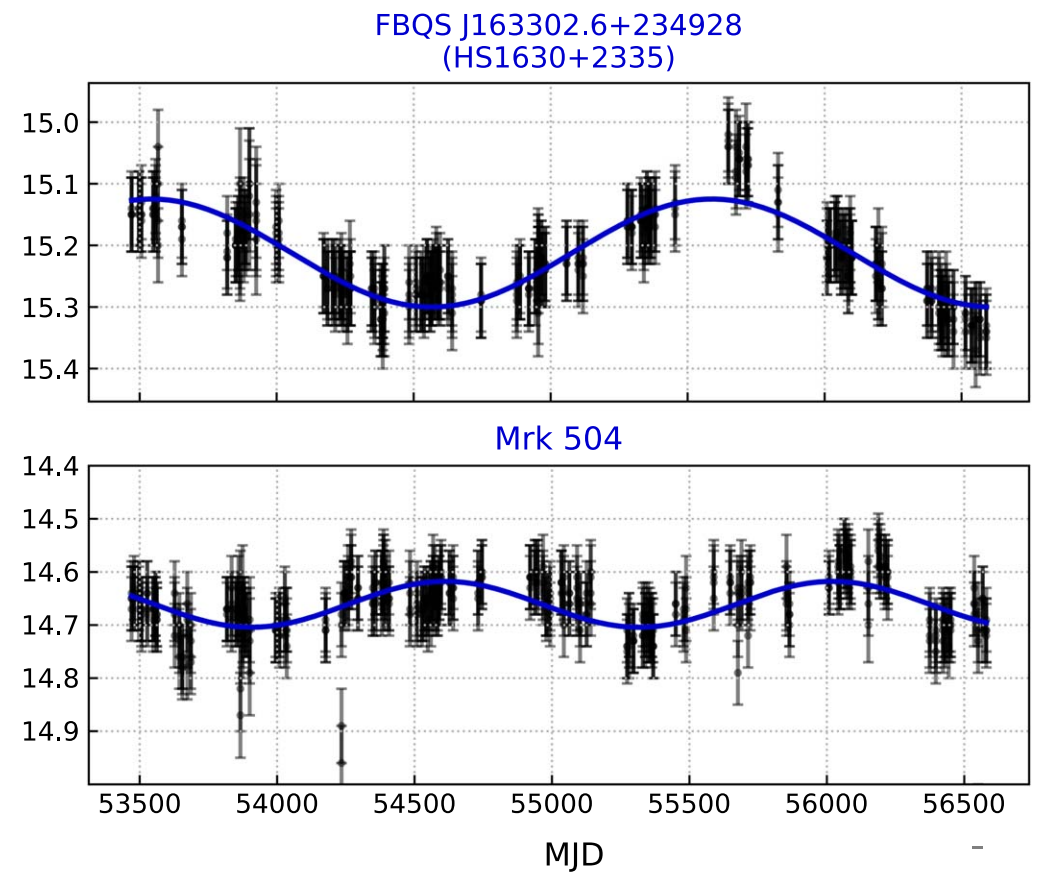


Figure 4. The optical periodic light curves of the HS1630+2335 (or FBQS J163302.6+234928 in Chandra X-ray) and Mrk 504. Their periodicity (blue) are fitted with minimized sum of squared residuals ≈6e-6 and 3e-7, respectively. The best-fit periods here are 2046 days and 1410 days, respectively. Mrk 504 is an excellent candidate to follow up with PTA observation to constrain its mass, since no other mass estimate are available.

periods. We can readily compute a mass upper limit by rearranging Equations (1) for the chirp mass. We also compute the strain needed for an S/N = 3 detection in Mrk 504's sky position using H19 (based on the NANOGrav 11 yr data) at $f_{gw} = 16.4$ nHz (corresponding to an orbital period of 1410), and find this to be $h < 4.4 \times 10^{-15}$. Using the source's distance of 160 Mpc, we can now constrain the chirp mass to be $\mathcal{M}_c < 1.4 \times 10^9 \, M_\odot$. Assuming an equal mass ratio, q = 1, we can limit the total mass of the binary to be $M < 3.3 \times 10^9 \, M_\odot$. Ho et al. (2008) uses the H I emission line method (Greene & Ho 2005) to find the BH mass of Mrk 504 (alternative name PG 1659+294), $\log(M_{\rm BH}/M_\odot) = 6.69 \pm 0.5$. Mrk 504 is also in the process of a reverberation mapping campaign (Lick AGN Monitoring Project), which could yield a more accurate mass estimate (Pancoast et al. 2019).

Furthermore, we independently compute the probability of each galaxy in CRTS hosting an SMBHB system emitting nanohertz GWs, as in Mingarelli et al. (2017). We find that 24 high-z AGN should not be able to host SMBHB systems at all (Table 4), because there has not been enough time for such binary systems to form under the assumption that they undergo a dynamical friction phase followed by a stellar hardening phase. The detection of GWs from one of these *unlikely* host galaxies would imply that significant gas interactions and/or binary eccentricity are accelerating these high-z mergers—a plausible scenario and a subject of future study—or that these periodic light curves are not truly tracing binary activity.

Importantly, we find that the existence of a GW background does not impede the detection of individual SMBHB at higher frequencies probed by CRTS, PTF, and others. Since the background is predominantly a very low-frequency GW signal, it only decreases our sensitivity by as factor of \sim 3.0 at \sim 11 nHz, the lowest frequency considered here.

7. Discussion

Our next step will be to analyze recent data from the Sloan Digital Sky Survey (SDSS; Liao et al. 2021) and Dark Energy Survey (DES; Chen et al. 2020). These further studies will be important, since with the CRTS, SDSS, and DES surveys, we may be able to find some common false-positive signals of binary activity if SMBHB candidates are completely ruled out by a lack of GW signal. Upcoming wide-field time-domain surveys such as the Rubin Observatory Legacy Survey of Space and Time (LSST; Ivezić et al. 2019), and ambitious spectroscopic surveys such as the Sloan Digital Sky Survey-V (SDSS-V; Kollmeier et al. 2017) and the Dark Energy Spectroscopic Instrument (DESI; Flaugher & Bebek 2014) will reveal a sky rich in potential SMBHBs systems (Kelley et al. 2019). Indeed, this work will form an important basis for assessing the credibility of SMBHB host galaxies that can be used in the LSST and SDSS-V era, when the sky is full of SMBHB candidates.

To this end, we outline general and concrete detection strategies can be initiated to make a GW detection from a candidate SMBHB host galaxy, or to rule out a given AGN as an SMBHB host galaxy. To optimize our ability to detect these GWs, we propose the following strategy for the CRTS

Table 4
Unlikely SMBHB Candidates When Computing the Probability of Each CRTS Candidate Hosting an SMBHB System via Equations (3)

Object Name	Z	$\log(M)$ $[M_{\odot}]$	Strain h_0	NG <i>ρ</i> , 11 yr	IPTA ρ, 2025	SKA1 ρ, 2030	SKA2 ρ, 2034+
SDSS J164452.71+430752.2	1.715	10.15	4.94E-16	0.65	3.67	13.77(6.26)	30.82(12.73)
SDSS J114857.33+160023.1	1.224	9.9	3.03E-16	0.22	1.39	6.88(2.74)	16(6.27)
HS 0926+3608	2.15	9.95	2.04E-16	0.08	0.74	4.29(1.66)	9.52(3.68)
SDSS J092911.35+203708.5	1.845	9.92	2.02E-16	0.07	0.87	4.43(1.73)	10.89(4.17)
SDSS J133516.17+183341.4	1.192	9.76	1.91E-16	0.18	1	4.67(1.92)	9.7(3.87)
SDSS J140704.43+273556.6	2.222	9.94	1.89E-16	0.17	0.95	4.5(1.86)	8.9(3.56)
SDSS J134855.27-032141.4	2.099	9.89	1.78E-16	0.14	0.8	4.09(1.64)	7.95(3.17)
SDSS J160730.33+144904.3	1.8	9.82	1.45E-16	0.17	0.95	3.97(1.71)	7.94(3.22)
SDSS J124119.04+203452.7	1.492	9.4	1.45E-16	0.09	0.63	3.2(1.29)	7.57(2.99)
SDSS J131706.19+271416.7	2.672	9.92	1.34E-16	0.11	0.63	3.08(1.26)	6.5(2.57)
QNZ3:54	1.402	9.27	7.34E-17	0.04	0.19	0.57(0.29)	1.59(0.66)
3C 298.0	1.437	9.57	6.73E-17	0.08	0.42	1.8(0.74)	3.99(1.6)
SDSS J083349.55+232809.0	1.155	9.4	6.73E-17	0.08	0.42	1.8(0.74)	3.99(1.6)
SDSS J155647.78+181531.5	1.502	9.51	6.24E-17	0.06	0.35	1.54(0.66)	2.91(1.18)
SDSS J094450.76+151236.9	2.118	9.61	6.00E-17	0.02	0.21	1.22(0.47)	2.64(1.01)
SDSS J121018.66+185726.0	1.516	9.53	5.82E-17	0.04	0.26	1.32(0.53)	2.94(1.15)
BZQJ0842+4525	1.408	9.48	5.02E-17	0.02	0.22	1.11(0.44)	2.82(1.09)
SDSS J121457.39+132024.3	1.494	9.46	4.25E-17	0.03	0.2	0.97(0.39)	2.33(0.92)
SDSS J082121.88+250817.5	1.906	9.53	4.18E-17	0.01	0.19	0.94(0.37)	2.4(0.92)
SDSS J093819.25+361858.7	1.677	9.32	2.85E-17	0.01	0.08	0.51(0.2)	1.08(0.42)
SDSS J165136.76+434741.3	1.604	9.34	2.45E-17	0.03	0.18	0.67(0.3)	1.47(0.61)
SDSS J014350.13+141453.0	1.438	9.21	1.99E-17	0.01	0.1	0.44(0.19)	0.95(0.41)
SDSS J123147.27+101705.3	1.733	9.2	1.34E-17	0.01	0.06	0.31(0.12)	0.71(0.28)
SDSS J080809.56+311519.1	2.642	8.36	4.34E-19	0	0	0.01(0)	0.02(0.01)

Notes. We found that 24 candidates were not viable binaries, though this may be due to the limitations of our model. For them to be viable, their parent galaxies would have had to start their mergers at z > 4, and furthermore one would need to invoke physical processes such as high eccentricity and strong accretion-based torques for the binaries to be emitting GWs at the time of observation.

candidates, which can be broadly applied to other such periodic AGN: (i) Start or maintain a high-cadence observing program for pulsars closely aligned with the top candidates in Table 1 (or any future candidate in general). If no such pulsars exist, ones can be added via pulsar searches (Roshi et al. 2019) or targeted radio follow-ups of Fermi-LAT unassociated sources (so far, ~20% of these have been added to NANOGrav⁸). (ii) Increase the amount of time spent observing these pulsars, to lower their rms white noise values. (iii) Combine pulsar data sets to achieve an immediate increase in cadence. (iv) Use targeted continuous GW searches to improve strain limits by a factor of at least two (Arzoumanian et al. 2020a).

These strategies have not been applied to candidates in Table 1 or Table 2, and could significantly accelerate their time to detection. Moreover, a new pulsar added via, e.g., Fermi is almost immediately valuable for continuous GW detection, as we showed in Figure 1 for the SKA.

Some particularly interesting candidates to watch are 3C66B, which could show GW frequency evolution; HS1630, where the mass can be constrained with upcoming IPTA observations; and Mrk 504, where we were able to compute a mass upper limit, $M = 3.3 \times 10^9~M_{\odot}$. In addition to the latter being relatively nearby at 160 Mpc, this rather good mass constraint could also be due to Mrk 504's proximity to pulsar J1713 +0747—an exceptional pulsar.

Large errors on the SMBH mass estimates from Shen et al. (2008) translate into large strain errors, since $h \propto [q/(1+q)^2]M^{5/3}$. Therefore, uncertainties in q will

always be subdominant to uncertainties in M (e.g., Figure 1). In fact, the SMBH masses may have been overestimated by a statistical factor of 3 (Sesana et al. 2018), due to the steep slope of the BH mass function at high mass. We are therefore very interested in investigating the differences between a systematic mass overestimate of a factor of 3 versus an error in a BH host galaxy scaling relation, in future work. We believe that our mass limits and the eventual detection of GWs from these systems will allow us to disentangle these competing mass errors

Indeed, PTAs offer a unique opportunity to constrain the chirp mass \mathcal{M}_c of candidate SMBHBs, which in turn provides new GW-based constraints on the underlying EM-based SMBH mass estimates (e.g., Shen et al. 2008). However, surveys like CRTS may select quasars exhibiting red noise that only appears to be periodic over a short time span (Vaughan et al. 2016). The detection strategies we outline, however, will allow us to identify *true* binary SMBHs by confirming and ruling out signals that are simply red noise, making this toolkit complementary to previous methods, e.g., Vaughan et al. (2016) and Kelley et al. (2019). Zhu & Thrane (2020)'s Bayesian approach to measuring periodicity is also a promising tool to mitigate this risk and identify truly periodic signals.

We previously discussed the limitations of Doppler boosting in identifying potentially detectable SMBHBs (D'Orazio et al. 2015)—such small mass ratios make detecting such binaries exceedingly difficult. However, in the case of PG1302-102, we allow ourselves to be cautiously optimistic. The strain of the candidate SMBHB in this galaxy is $h \sim 9 \times 10^{-18}$ at ~ 14 nHz (Graham et al. 2015b). Using the detection strategies we describe here, complemented by a targeted search for the

https://confluence.slac.stanford.edu/display/GLAMCOG/Public+List +of+LAT-Detected+Gamma-Ray+Pulsars

additional factor of two (Arzoumanian et al. 2020a) from performing a targeted GW search, may make it detectable with SKA2. Additionally, D'Orazio et al. (2015) and Noble et al. (2021) use hydrodynamical simulations to demonstrate that SMBH binaries with more equal mass ratios, $q \gtrsim 0.3$, which is the adopted assumption in our calculation of strains (0.25 < q < 1), show EM periodicity at orbital periods a factor of a \sim few shorter due to an overdensity in the circumbinary disk. This would generally result in larger strains than in our predictions.

Some 24 high-mass, high-z AGN in CRTS are not viable candidates according to our SMBHB evolution models: the host galaxies would have had to merge at z > 4 to give rise to these binaries, and our current methodologies only extend to z = 4 due to limitations in Illustris (Rodriguez-Gomez et al. 2015). Moreover, the SMBH occupation fraction for the parent galaxies that formed the current binaries would have to be 1.0 at z > 4, which would also be an interesting result. Our models do not, however, include gas and potential binary eccentricity, both of which would make the binaries evolve more quickly. A GW detection from one of these 24 host galaxies, such as SDSS J164452+4307 (detectable by IPTA in 2025; see Table 2), could therefore inform SMBHB evolution models, and may help in understanding the origins of SMBHs seeds (Volonteri et al. 2008; Tanaka & Haiman 2009) and their occupation fraction.

Importantly, we found that the presence of a stochastic GW background does not impede our detection prospects. In fact, if these AGN really are SMBHB systems, they may induce some anisotropy in the GW background (Mingarelli et al. 2013, 2017). Detection of anisotropy will likely follow that of the isotropic GW background in the next few years.

So far, no CGWs have been detected at any frequency from any compact object. Long-lived CGWs are currently detectable with PTAs, and may eventually be complemented by astrometric GW detection (Moore et al. 2017). Given that SMBHBs in the PTA band will stay in-band for tens of millions of years, the current periodic light curves in CRTS, PTF, and PAN-STARRS1 offer us a unique opportunity to study SMBHB host galaxies and their EM emissions. Identifying these EM emissions will be invaluable information for the Laser Interferometer Space Antenna (LISA; Baker et al. 2019), where the angular resolution is relatively poor and the signals will only last weeks to months. Understanding the expected EM emissions from SMBHB host galaxies is thus important groundwork to lay for both PTAs and LISA in this new era of multimessenger astrophysics.

The authors thank William Garnier for an updated SKA1 timeline, and Zoltán Haiman, Maria Charisi, Michael Lam, M. Lynne Saade, Alberto Sesana, Yacine Ali-Haïmoud, Thomas McCausland, and Sean Oh for useful discussions. CMFM thanks G. S. C. Mingarelli, B. A. Lee, A. MacKenzie, A. von Hirschberg, D. Bergin for their invaluable support during lockdown. The Flatiron Institute is supported by the Simons Foundation. The NANOGrav project receives support from National Science Foundation (NSF) PIRE program award number 0968296 and NSF Physics Frontier Center award number 1430284. C.X. was supported by NASA ADAP grant NNX17AL82G.

Software: Astropy (Astropy Collaboration et al. 2013, 2018), Hasasia (Hazboun et al. 2019a), Healpy (Zonca et al. 2019),

Matplotlib (Hunter 2007), Numpy (van der Walt et al. 2011), Pandas (McKinney 2010), SciPy (Virtanen et al. 2020), NanohertzGWs (Mingarelli 2017).

ORCID iDs

Chengcheng Xin https://orcid.org/0000-0003-3106-8182 Chiara M. F. Mingarelli https://orcid.org/0000-0002-4307-1322

Jeffrey S. Hazboun https://orcid.org/0000-0003-2742-3321

References

```
Aggarwal, K., Arzoumanian, Z., Baker, P. T., et al. 2019, ApJ, 880, 116
Albareti, F. D., Prieto, C. A., Almeida, A., et al. 2017, ApJS, 233, 25
Antonucci, R. 1993, ARA&A, 31, 473
Arzoumanian, Z., Baker, P. T., Blumer, H., et al. 2020b, ApJL, 905, L34
Arzoumanian, Z., Baker, P. T., Brazier, A., et al. 2018a, ApJ, 859, 47
Arzoumanian, Z., Baker, P. T., Brazier, A., et al. 2020a, ApJ, in press
   (arXiv:2005.07123)
Arzoumanian, Z., Brazier, A., Burke-Spolaor, S., et al. 2018b, ApJS, 235, 37
Babak, S., Petiteau, A., Sesana, A., et al. 2016, MNRAS, 455, 1665
Babak, S., & Sesana, A. 2012, PhRvD, 85, 044034
Baker, J., Bellovary, J., Bender, P. L., et al. 2019, arXiv:1907.06482
Baskaran, D., Polnarev, A., Pshirkov, M., & Postnov, K. 2008, PhRvD, 78,
Bécsy, B., & Cornish, N. J. 2020, CQGra, 37, 135011
Begelman, M. C., Blandford, R. D., & Rees, M. J. 1980, Natur, 287, 307
Bonetti, M., Sesana, A., Barausse, E., & Haardt, F. 2018, MNRAS, 477, 2599
Boyle, L., & Pen, U.-L. 2012, PhRvD, 86, 124028
Burke-Spolaor, S., Taylor, S. R., Charisi, M., et al. 2019, A&ARv, 27, 5
Burt, B. J., Lommen, A. N., & Finn, L. S. 2011, ApJ, 730, 17
Chamberlin, S. J., & Siemens, X. 2012, PhRvD, 85, 082001
Charisi, M., Bartos, I., Haiman, Z., et al. 2016, MNRAS, 463, 2145
Charisi, M., Haiman, Z., Schiminovich, D., & D'Orazio, D. J. 2018, MNRAS,
Chen, Y.-C., Liu, X., Liao, W.-T., et al. 2020, MNRAS, 21, 1
D'Orazio, D. J., & Haiman, Z. 2017, MNRAS, 470, 1198
D'Orazio, D. J., Haiman, Z., Dufell, P., Farris, B. D., & MacFadyen, A. I.
   2015, MNRAS, 452, 2540
D'Orazio, D. J., Haiman, Z., Duffell, P., MacFadyen, A., & Farris, B. 2016,
     NRAS, 459, 2379
D'Orazio, D. J., Haiman, Z., & Schiminovich, D. 2015, Natur, 525, 351
Ellis, J. A., Siemens, X., & Creighton, J. D. E. 2012, ApJ, 756, 175
Farris, B. D., Duffell, P., Macfadyen, A. I., & Haiman, Z. 2014a, ApJ, 783, 12
Farris, B. D., Duffell, P., MacFadyen, A. I., & Haiman, Z. 2014b, MNRAS,
  447, L80
Flaugher, B., & Bebek, C. 2014, Proc. SPIE, 9147, 91470S
Goulding, A. D., Greene, J. E., Bezanson, R., et al. 2018, PASJ, 70, S37
Graham, M. J., Djorgovski, S. G., Stern, D., et al. 2015a, MNRAS, 453, 1562
Graham, M. J., Djorgovski, S. G., Stern, D., et al. 2015b, Natur, 518, 74
Greene, J. E., & Ho, L. C. 2005, ApJ, 630, 122
Hazboun, J., Romano, J., & Smith, T. 2019a, JOSS, 4, 1775
Hazboun, J. S., Romano, J. D., & Smith, T. L. 2019b, PhRvD, 100, 104028
Hellings, R. W., & Downs, G. S. 1983, ApJL, 265, L39
Ho, L. C., Darling, J., & Greene, J. E. 2008, ApJS, 177, 103
Hulse, R. A., & Taylor, J. H. 1975, ApJL, 195, L51
Hunter, J. D. 2007, CSE, 9, 90
Jun, H. D., Stern1, D., Graham, M. J., et al. 2015, ApJL, 814, L12
Ivezić, Ž., Kahn, S. M., Tyson, J. A., et al. 2019, ApJ, 873, 111
Kauffmann, G., & Haehnelt, M. 2000, MNRAS, 311, 576
Keane, E., Bhattacharyya, B., Kramer, M., et al. 2015, in Advancing
   Astrophysics with the Square Kilometre Array (AASKA14), 215 (Trieste:
   SISSA), PoS(AASKA14)0402015aska.confE..40K
Kelley, L., Charisi, M., Burke-Spolaor, S., et al. 2019, BAAS, 51, 490
Kollmeier, J. A., Zasowski, G., Rix, H.-W., et al. 2017, arXiv:1711.03234
Krolik, J. H., & Begelman, M. C. 1988, ApJ, 329, 702
Laine, S., Dey, L., Valtonen, M., et al. 2020, ApJL, 894, L1
Lam, M. T. 2018, ApJ, 868, 33
Lam, M. T., Cordes, J. M., Chatterjee, S., et al. 2016, ApJ, 819, 155
Lam, M. T., McLaughlin, M. A., Arzoumanian, Z., et al. 2019, ApJ, 872, 193
Lehto, H. J., & Valtonen, M. J. 1996, A&A, 460, 207
Liao, W.-T., Chen, Y.-C., Liu, X., et al. 2021, MNRAS, 500, 4025
```

Liu, T., Gezari, S., Ayers, M., et al. 2019, ApJ, 884, 36

```
McKinney, W. 2010, in Proc. of the 9th Python in Science Conf., ed.
   S. van der Walt & J. Millman (USA: SciPy), 56
Milosavljević, M., & Merritt, D. 2001, ApJ, 563, 34
Mingarelli, C. 2017, ChiaraMingarelli/nanohertz_GWs: First release!, v1.0,
  Zenodo, doi:10.5281/zenodo.838712
Mingarelli, C. M., Lazio, T. J. W., Sesana, A., et al. 2017, NatAs, 1, 886
Mingarelli, C. M. F., & Sidery, T. 2014, PhRvD, 90, 062011
Mingarelli, C. M. F., Sidery, T., Mandel, I., & Vecchio, A. 2013, PhRvD, 88,
Moore, C. J., Mihaylov, D. P., Lasenby, A., & Gilmore, G. 2017, PhRvL, 119,
   261102
Noble, S. C., Krolik, J. H., Campanelli, M., et al. 2021, arXiv:2103.12100
O'Beirne, L., Cornish, N. J., Vigeland, S. J., & Taylor, S. R. 2019, PhRvD, 99,
Pancoast, A., Skielboe, A., Pei, L., et al. 2019, ApJ, 871, 108
Perera, B. B. P., DeCesar, M. E., Demorest, P. B., et al. 2019, MNRAS,
  490, 4666
Astropy Collaboration, Price-Whelan, A. M., Sipőcz, B. M., et al. 2018, AJ,
   156, 123
Ouinlan, G. D. 1996, NewA, 1, 35
Astropy Collaboration, Robitaille, T. P., Tollerud, E. J., et al. 2013, A&A,
   558, A33
```

Rodriguez-Gomez, V., Genel, S., Vogelsberger, M., et al. 2015, MNRAS,

449, 49

```
Roedig, C., Krolik, J. H., & Miller, M. C. 2014, ApJ, 785, 115
Roshi, A., Anderson, L. D., Araya, E., et al. 2019, BAAS, 51, 244
Ryan, G., & MacFadyen, A. 2017, ApJ, 835, 199
Ryu, T., Perna, R., Haiman, Z., Ostriker, J. P., & Stone, N. C. 2018, MNRAS,
  473, 3410
Saade, M. L., Stern, D., Brightman, M., et al. 2020, ApJ, 900, 148
Sesana, A. 2013, CQGra, 30, 224014
Sesana, A., Haiman, Z., Kocsis, B., & Kelley, L. Z. 2018, ApJ, 856, 42
Shannon, R. M., Osłowski, S., Dai, S., et al. 2014, MNRAS, 443, 1463
Shen, Y., Greene, J. E., Strauss, M. A., Richards, G. T., & Schneider, D. P.
  2008, ApJ, 680, 169
Sudou, H., Iguchi, S., Murata, Y., & Taniguchi, Y. 2003, Sci, 300, 1263
Tanaka, T., & Haiman, Z. 2009, ApJ, 696, 1798
Taylor, S., Ellis, J., & Gair, J. 2014, PhRvD, 90, 104028
Tiede, C., Zrake, J., MacFadyen, A., & Haiman, Z. 2020, ApJ, 900, 11
van der Walt, S., Colbert, S. C., & Varoquaux, G. 2011, CSE, 13, 22
Vaughan, S., Uttley, P., Markowitz, A. G., et al. 2016, MNRAS, 461, 3145
Virtanen, P., Gommers, R., Oliphant, T. E., et al. 2020, NatMe, 17, 261
Volonteri, M., Lodato, G., & Natarajan, P. 2008, MNRAS, 383, 1079
Xin, C., Charisi, M., Haiman, Z., & Schiminovich, D. 2020, MNRAS,
  495, 1403
Zhu, X.-J., Cui, W., & Thrane, E. 2019, MNRAS, 482, 2588
Zhu, X.-J., & Thrane, E. 2020, ApJ, 900, 117
Zonca, A., Singer, L., Lenz, D., et al. 2019, JOSS, 4, 1298
```